Check for updates

ChemSystemsChem

Chemistry Europe
European Chemical Societies Publishing

Accepted Article

Title: Tuning the Kinetic Trapping in Chemically Fueled Self-Assembly

Authors: Brigitte A. K. Kriebisch, Christine M. E. Kriebisch, Alexander M. Bergmann, Caren Wanzke, Marta Tena-Solsona, and Job Boekhoven

This manuscript has been accepted after peer review and appears as an Accepted Article online prior to editing, proofing, and formal publication of the final Version of Record (VoR). The VoR will be published online in Early View as soon as possible and may be different to this Accepted Article as a result of editing. Readers should obtain the VoR from the journal website shown below when it is published to ensure accuracy of information. The authors are responsible for the content of this Accepted Article.

To be cited as: *ChemSystemsChem* **2022**, e202200035

Link to VoR: https://doi.org/10.1002/syst.202200035

WILEY-VCH

25704206, ja, Downloaded from https://chemistry-europe.onlinelibrary.wiley.com/doi/10.1002/syst.202200035 by Cochrane Germany, Wiley Online Library on [13/10/2022]. See the Terms and Conditions (https://onlinelibrary.wiley.com/terms-and-conditions) on Wiley Online Library for rules of use; OA articles are governed by the applicable Creative Commons License

10.1002/syst.202200035

WILEY-VCH

RESEARCH ARTICLE

Tuning the Kinetic Trapping in Chemically Fueled Self-Assembly.

Brigitte A. K. Kriebisch[+], Christine M. E. Kriebisch[+], Alexander M. Bergmann, Caren Wanzke, Marta Tena-Solsona, Job Boekhoven*

[*] B. A. K. Kriebisch[+], C. M. E. Kriebisch[+], A. M. Bergmann, Dr. C. Wanzke, Dr. M. Tena-Solsona, Prof. Dr. J. Boekhoven*
School of Natural Science, Department of Chemistry, Technische Universität München
Lichtenbergstraße 4, 85748 Garching b. München (Germany),
E-Mail job.boekhoven@tum.de
[+] These authors contributed equally to this work.
Supporting information and the ORCID identification number(s) for the author(s)of this article can be found under

Abstract: Nature uses dynamic, molecular self-assembly to create cellular architectures that adapt to their environment. For example, a guanosine triphosphate (GTP)-driven reaction cycle activates and deactivates tubulin for dynamic assembly into microtubules. Inspired by dynamic self-assembly in biology, recent studies have developed synthetic analogs of assemblies regulated by chemically fueled reaction cycles. A challenge in these studies is to control the interplay between rapid disassembly and kinetic trapping of building blocks known as dynamic instabilities. In this work, we show how molecular design can tune the tendency of molecules to remain trapped in their assembly. We show how that design can alter the dynamic of emerging assemblies. Our work should give design rules for approaching dynamic instabilities in chemically fueled assemblies to create new adaptive nanotechnologies.

Introduction

In molecular self-assembly, molecules are designed to interact with one another to form larger, supramolecular complexes.[1] The assembly process alters the material properties of the system, which gives rise to supramolecular materials.[2] Recently, there has been a focus on dynamic supramolecular materials, *i.e.*, materials that change and adapt to their environment.[3] In such materials, molecules are designed to assemble or disassemble in response to a trigger. For example, peptides can be designed to assemble or disassemble upon enzymatic phosphorylation, dephosphorylation, or an increase in pH.[4] In these dynamic assembly mechanisms, kinetic traps can trap molecules in their assembly because the thermal energy available is insufficient to overcome the energy barrier for disassembly.[5] As molecules and their assembly become increasingly more complex; it becomes more challenging to predict whether such unwanted kinetic trapping will occur.

Chemically fueled self-assembly is an extreme case of dynamic self-assembly.[6] Here, assembly is coupled to a chemical reaction cycle to yield assemblies regulated through the kinetics of that reaction cycle. The reaction cycle comprises at least two chemical reactions, *i.e.*, an activation reaction that activates building blocks for self-assembly at the expense of a high-energy chemical reagent (*i.e.*, a chemical fuel) and a spontaneous deactivation reaction that reverts the building blocks to their precursor state (Scheme 1A). In dynamic self-assembly of, for example, tubulin or actin, the emerging assemblies have vastly different properties compared to their in-equilibrium analogs because building blocks are constantly activated and deactivated for assembly.[7] When the assembly and disassembly rates of building blocks are fast, the assemblies can be dynamic (Scheme 1B).

In contrast, when the disassembly of the precursor is slow, the molecules remain trapped in the assembled state and can reactivate before disassembly. Such a situation results in chemically fueled self-assembly without the dynamics of assembly and disassembly. It is thus, to a lesser degree, regulated by the kinetics of the reaction cycle (Scheme 1C).

Dynamic instabilities of microtubules are a result of the delicate interplay between trapping and rapid disassembly of deactivated building blocks. Building blocks in microtubules are rapidly deactivated but do not disassemble immediately. Only when the tubule's endcap becomes unstable due to faster deactivation than building block assembly, the tubule enters the catastrophe phase and rapidly disassemble the trapped building blocks. Thus, kinetic trapping of building blocks can offer unwanted lag in disassembly, but it can also offer exciting opportunities to engineer dynamic instabilities. Therefore, controlling the degree of kinetic trapping of building blocks in assemblies could open the door to engineer fibers that rapidly disassemble, treadmill, or display other behavior typically observed in biology.

Tuning the degree of kinetic trapping of molecules is challenging because the mechanisms of kinetic trapping are poorly understood. Here, we show how molecular design influences the degree of kinetic trapping in chemical-fueled dynamic self-assemblies and thus the dynamic behavior of the self-assemblies.

This article is protected by copyright. All rights reserved.

25704206, ja, Downloaded from https://chemistry-europe.onlinelibrary.wiley.com/doi/10.1002/syst.202200035 by Cochrane Germany, Wiley Online Library on [13/10/2022]. See the Terms and Conditions (https://onlinelibrary.wiley.com/terms-and-conditions) on Wiley Online Library for rules of use; OA articles are governed by the applicable Creative Commons License

Accepted Manuscript

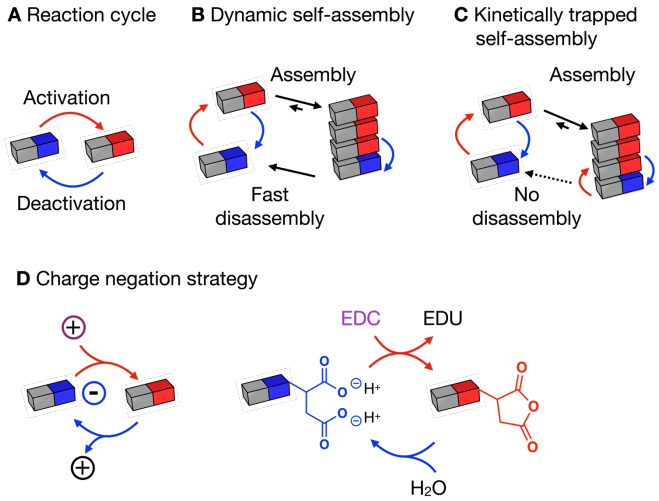

Scheme 1. A) Scheme of a fuel-driven reaction cycle. Red arrows depict fuel-driven activation reactions. Blue arrows depict spontaneous deactivation reactions. **B)** In chemically fueled, dynamic self-assembly, the activated building block should assemble while the deactivated building block disassembles. **C)** In kinetically trapped assemblies, disassembly does not follow deactivation. Building blocks get reactivated in the assembly. **D)** Transient negation of charges by the reaction cycle can be applied to drive self-assembly. EDC-driven reaction cycle negates the charges on a dicarboxylate.

To create chemically fueled assemblies, we and others used a strategy in which a chemical reaction cycle transiently negates the charges on a molecule (Scheme 1D).[7-9] Upon activation, an anionic, well-soluble precursor becomes charge-neutral, which induces product assembly. The deactivation occurs while the building block is assembled; it reinstates the negative charges and thus leads to its disassembly. We described a reaction cycle driven by the hydration of the condensing agent EDC (1-ethyl-3-(3-dimethyl aminopropyl)carbodiimide, Scheme 1D).[8b] In the activation, EDC reacts with an anionic dicarboxylate precursor to form its corresponding uncharged anhydride (product). In the deactivation, the product hydrolyzes to yield the dicarboxylate precursor. The anhydride precursor has a half-life of tens of seconds before deactivation. The removal of the charges of the anionic dicarboxylate can induce self-assembly. *Vice versa*, the deactivation converts the non-charged anhydride to its corresponding dicarboxylate *via* hydrolysis and yields the charged precursors, which induces disassembly.

Using the charge abolishment approach has resulted in assemblies with dynamic behavior like vesicles[9g], coacervates[9e], and oil droplets[10]. However, not all fueled assemblies formed through charge negation are dynamic. In some cases, chemically fueled self-assembly into fibers results in slow disassembly or even kinetically trapped assemblies.[8, 9f] In other words, the dynamics of the reaction cycle are fast, but the dynamics of assembly and disassembly are not. Furthermore, because the mechanisms of kinetic trapping are not understood, it is challenging to predict or design molecules that form dynamic assemblies.

In this work, we study the mechanism of kinetically trapping in chemically fueled fibers regulated through transient charge negation. We find that the assembly increases the peptide's apparent pK_a, which implies that the molecule remains protonated upon deactivation. In its protonated, uncharged state, the charge-charge repulsion with neighboring deactivated precursors is negligible, which explains why the disassembly is slow, and precursors remain trapped. We believe this mechanism is generalizable for the disassembly of other peptides based on charge-charge repulsion.[8a, 9q, 11] We also provide solutions to overcome the trapping of the precursor in the fibers, which yield chemically fueled fibers with increased dynamics.

Results and Discussion

Molecular design controls kinetic trapping

We used the tripeptides Fmoc-GGD and Fmoc-AVD (Fig. 1A, B), where G is the amino acid glycine, A is the amino acid alanine, V is the amino acid valine, and D stands for aspartic acid. These peptides are dissolved at 10 mM in an aqueous buffer of MES at pH 6.0. A Nile Red assay found no evidence of assembly, confirming that these peptides were well-dissolved in their precursor state (Fig. 1C, D, Fig. S1). Adding 100 mM EDC to these precursor solutions initiated the reaction cycle. It led to the formation of a turbid solution and a turbid hydrogel for Fmoc-GGD and Fmoc-AVD, respectively. Notably, the turbidity by Fmoc-GGD was transient and faded as the reaction cycle had consumed all fuel. In contrast, the hydrogel of Fmoc-AVD was not transient and remained intact far after all fuel was consumed (Fig. 1C-F). Confocal microscopy was used to study the morphology of the assembly and found, in line with previous work, that Fmoc-GGD formed transient vesicles (Fig. 1C, Fig. S2A).[8b] In contrast, Fmoc-AVD assembled into fibers (Fig. 1D, Fig. S2B).[9g] We studied the evolution of the reaction cycle by applying fuel, and at predetermined time points, we used a benzylamine quench[12] to stop the reaction cycle and measure its contents by HPLC (Fig. 1E, F). The anhydride product was temporarily present, and, as the system ran out of fuel, the product disappeared.

To assess the dynamics of the assembly and disassembly process, the turbidity of the solution in response to EDC was followed in a plate reader (Fig. 1E, F). While the Fmoc-GGD-based vesicles dissolved to yield a transparent solution as the product concentration decayed, the fibers by Fmoc-AVD did not. After 24 hours, a substantial amount of turbidity was observed for Fmoc-AVD, even though all anhydride had hydrolyzed within the first hour of the reaction cycle. From this observation, it is clear that the precursor remained kinetically trapped in the fibers.

Using ^{1}H-NMR spectroscopy, the assembly's composition was measured as a function of time. We used the fact that peptides in an assembly do not show NMR signals. We can thus measure how much of the 10 mM initial peptide resides in the assemblies. Combined with the concentrations of the activated product as determined by HPLC, we could thus determine the ratio of precursor and product in the assemblies. Here we assume that all activated product is in the assemblies. Three minutes after the addition of EDC, we found that both the fibers and the vesicles were composed of a coassembly of precursor and product (Fig. S3). However, 24 hours after starting the reaction cycle, ^{1}H-NMR shows us the initial peptide concentration in the case of Fmoc-GGD, which points to complete disassembly.

In contrast, for Fmoc-AVD, roughly 4.3 mM precursor remained kinetically trapped in assemblies after 24 hours (Fig. 1G). The kinetically trapped precursor was disassembled only when we heated the kinetically trapped Fmoc-AVD at 95°C for 5 min (Fig. S4). Finally, we supported our finding that Fmoc-AVD is kinetically trapped by a Nile Red assay. The Nile Red emission remained

This article is protected by copyright. All rights reserved.

25704206, ja, Downloaded from https://chemistry-europe.onlinelibrary.wiley.com/doi/10.1002/syst.202200035 by Cochrane Germany, Wiley Online Library on [13/10/2022]. See the Terms and Conditions (https://onlinelibrary.wiley.com/terms-and-conditions) on Wiley Online Library for rules of use; OA articles are governed by the applicable Creative Commons License

Accepted Manuscript

high for Fmoc-AVD, whereas no emission signal was visible for Fmoc-GGD after 24 hours (Fig. 1 H).

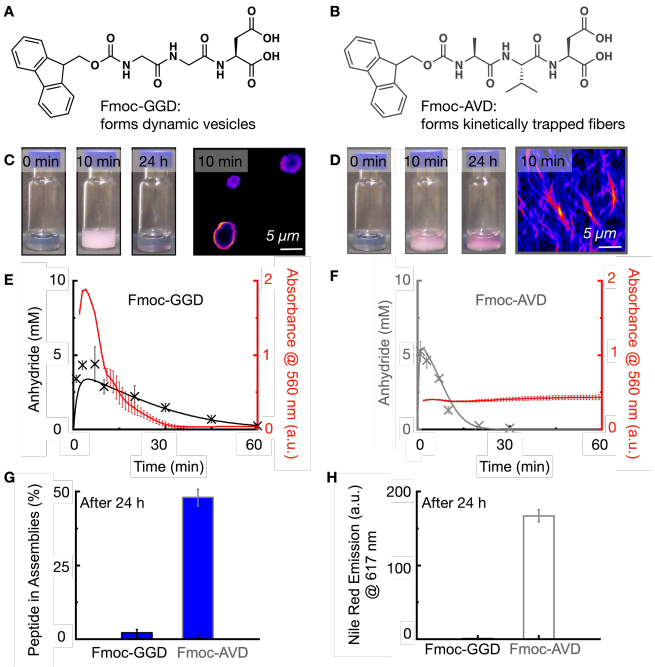

Figure 1. Peptide design controls kinetic trapping after the application of fuel. **A-B)** Molecular structure of Fmoc-GGD and Fmoc-AVD. **C-D)** Photographs and confocal micrographs, after fueling **C)** Fmoc-GGD and **D)** Fmoc-AVD with EDC, stained with Nile Red dye. **E-F)** Indication of correlation between the assembly process and the kinetics by measuring the anhydride formation (black markers) and the absorbance at 560 nm (solid red line) when fueling **E)** Fmoc-GGD, and **F)** Fmoc-AVD with EDC, stained with Nile Red dye. A kinetic model fits the experimental data (solid black line, Supporting Notes). **G)** The percentage of trapped precursor in the molecular assemblies after 24 hours, when fueling Fmoc-GGD, and Fmoc-AVD with EDC as determined by ^{1}H-NMR spectroscopy. **H)** Maximum emission intensity of Nile Red (a.u.) at 617 nm, 24 hours after fueling Fmoc-GGD (hardly visible), and Fmoc-AVD with EDC. All error bars are the standard deviation of the mean (n = 3).

The mechanism that kinetically traps precursors

We use a charge abolishment strategy in the design of the chemically fueled assemblies. We reasoned that upon hydrolysis of non-charged anhydrides, the negatively charged precursors repel each other and drive the disassembly. Based on the above data, this is not the case. We hypothesized that the precursor in the assembly might not be as anionic as we initially suspected. Upon deactivation of the product in a fiber of Fmoc-AVD, the negative charges on the precursor's carboxylate are not reinstated. This mechanism is induced by a drastic shift in the pK_a in the microenvironment of the fiber.[9f] It is well known that hydrophobic environments, *e.g.*, in peptide-based self-assembly or folding of proteins, shift the pK_a of aspartic and glutamic acid residues.[13] The hydrophobic microenvironment changes the dielectric constant of its medium, and thus the pK_a.[13c] In other words, the precursor in the solution is deprotonated, which prevents its assembly. However, the precursor in the fiber remains (partially) protonated and thus charge neutral and unable to disassemble (Fig. 2A). We measured the apparent pK_a of the Fmoc-AVD, and Fmoc-GGD and compared Ac-FAVD, a peptide that does not assemble and has apparent pK_a's of 2.2 and 4.2 (Fig. 2A, Fig. S5A). For Fmoc-GGD, we found only one apparent pK_a at 4.4 by titration of HCl (Fig. S5B). Interestingly, the solution turned turbid when the pH was close to the apparent pK_a. In other words, the measured apparent pK_a was of the precursor in an assembled state, likely different from the apparent pK_a of the precursor in solution. In contrast, for Fmoc-AVD, we found an apparent pK_a of 5.8, *i.e.*, far higher than the non-assembling Ac-FAVD (Fig. 2A, Fig. S5C).

As we carry out our chemically fueled reaction cycle at pH 6.0, it is reasonable to assume that most of the precursor of Fmoc-GGD in the solution or the vesicles is completely deprotonated. In the case of Fmoc-AVD, the apparent pK_a in the fibers is close to experimental conditions, implying that, on average, ~60% of the carboxylates were deprotonated. Consequently, the driving force of disassembly, *i.e.*, the accumulation of negative charges on the precursor, is far less prevalent on Fmoc-AVD than Fmoc-GGD. To further corroborate that hypothesis, we monitored the chemically fueled fibers by confocal microscopy in combination with Hoechst dye 33258. That dye is cationic and stains anionic assemblies like proteins and peptides, enabling us to monitor the accumulation of negative charges (Fig. S6).[14] We found that Hoechst 33258 colocalized with the vesicles formed by Fmoc-GGD throughout the reaction cycle (Fig. 2B). In contrast, the fibers formed by Fmoc-AVD hardly incorporated some Hoechst 33258 dye in the beginning of the reaction cycle, when deactivation is at its highest. After 10 min, the Hoechst 33258 signal was very faint or not observable, from which we conclude that the fibers are hardly anionic, which corroborates our earlier findings (Fig. 2B). Finally, we performed the exact same experiments as described above, but at various pH values between pH 6.0 and 6.5. ^{1}H-NMR showed a clear trend that less precursor got trapped with increasing pH, further corroborating that the surrounding media's pH is insufficient to deprotonate the kinetically trapped precursor (Fig. 2C, Fig. S7-9). We assume that working above pH 6.5 further avoids the kinetic trapping of precursor. However, at pH 7 or higher, we observed the formation of significant amounts of the side product N-acylisourea and much less anhydride.

The flat packing of β-sheets is responsible for the pK_a-shift

We explain the pK_a difference between assemblies of Fmoc-AVD and Fmoc-GGD by valine's high propensity to form flat ß-sheets compared to glycine. The formation of these flat β-sheets implies that the C-terminal aspartic acids are packed in a relatively high density which is well-known to shift pK_as.[13a, 13c] We measured the assembly's ability to bind Thioflavin (ThT), which measures the flatness of β-sheets, and also indicates the formation of gels.[15] We thus performed the ThT assay at a concentration, where fueling does not result in gel formation. We measured a high ThT signal when we fueled Fmoc-AVD with EDC, while we found no significant emission of ThT when we fueled Fmoc-GGD with EDC (Fig. 2D). Fourier-Transform Infrared Spectroscopy (FT-IR) revealed that both peptides had two predominant peaks around 1690 cm^{-1} and 1630 cm^{-1}, which we assign to the Fmoc-OCNH band and the amide I band (Fig. 2E). The amide I band (carbonyl stretch vibration) is particularly sensitive to hydrogen bonding in the peptide assembly.[16] For Fmoc-AVD, this peak was located at 1632 cm^{-1} and relatively sharp, which is indicative of elements of β-sheet (1625 cm^{-1}– 1640 cm^{-1}).[17] The same peak for Fmoc-GGD broadened drastically and shifted towards the region of 1650 cm^{-1}, which points towards elements of a random coil (1640 cm^{-1}– 1650 cm^{-1}).[17] The FT-IR data further corroborate that Fmoc-GGD is mainly engaged in random coil hydrogen bonds, whereas flat β-sheets are present in Fmoc-AVD assemblies. These flat β-sheets pack the carboxylates closely such that their pK_as shift.

This article is protected by copyright. All rights reserved.

25704206, ja, Downloaded from https://chemistry-europe.onlinelibrary.wiley.com/doi/10.1002/syst.202200035 by Cochrane Germany, Wiley Online Library on [13/10/2022]. See the Terms and Conditions (https://onlinelibrary.wiley.com/terms-and-conditions) on Wiley Online Library for rules of use; OA articles are governed by the applicable Creative Commons License

Accepted Manuscript

10.1002/syst.202200035

WILEY-VCH

RESEARCH ARTICLE

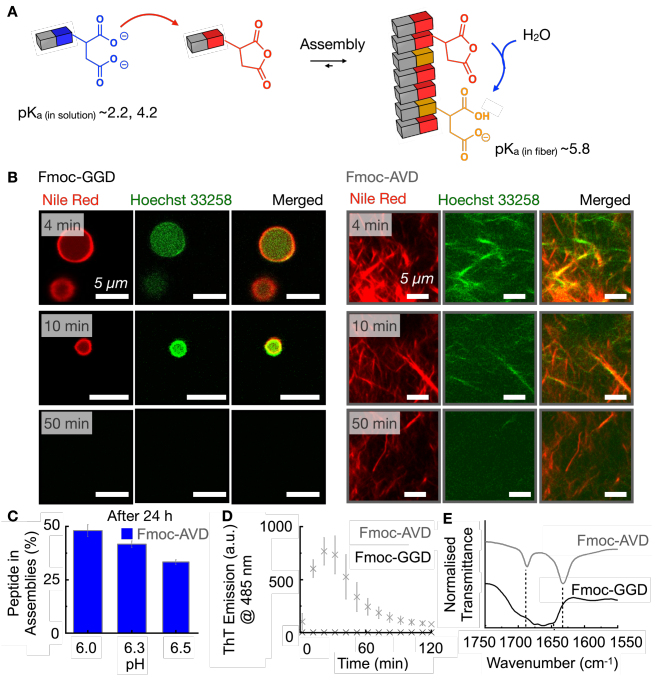

Figure 2. The mechanism of kinetic trapping. **A)** The pK_a of aspartic acid depends strongly on its microenvironment. **B)** Confocal micrographs after fueling Fmoc-GGD and Fmoc-AVD, stained with Nile Red and Hoechst 33258 dye, respectively. **C)** The percentage of trapped precursor in the molecular assemblies after 24 hours when Fmoc-AVD were fueled at pH 6, pH 6.3, and pH 6.5 as determined by ^{1}H-NMR spectroscopy. **D)** ThT fluorescence intensity at 485 nm over time as a measure of the presence of β-sheets when Fmoc-AVD or Fmoc-GGD are fueled with EDC. **E)** FT-IR spectra of Fmoc-AVD or Fmoc-GGD fueled with EDC at 3 min. The Fmoc-OCNH band at 1687 cm^{-1} and amide I band at 1632/1647 cm^{-1} (typical β-sheet/random coil) for Fmoc-AVD/Fmoc-GGD. All error bars represent the standard deviation of the mean for n = 3.

To test which of the amides in the peptide contributed to the organization of the C-termini and thus the shift in pK_a and kinetic trapping, we synthesized Fmoc-AVD(NMe) (Fig. 3). This compound is similar to Fmoc-AVD but lacks the last NH-bond due to methylation, which shifted the apparent pK_a from 5.8 back to 4.2 (Fig. 3, Fig. S10). In other words, the pK_a-shift upon self-assembly had disappeared entirely. Furthermore, transient aggregates emerge when fueling 10 mM Fmoc-AVD(NMe) with 100 mM EDC (Fig. S11A, B). ^{1}H-NMR and HPLC studies on the reaction cycle of Fmoc-AVD(NMe) showed a complete lack of coassembly of the precursor and thus no kinetic trapping (Fig. S11C, D). In other words, methylation of this crucial amide means that the precursor does not coassemble, and we can recover the dynamic character of the chemically fueled self-assembly.

Compound	*H-bonding interaction*	*Apparent pK_a*	
Fmoc-AVD(NMe)	Non	~ 4.2 ± 0.1 ~ 4.2 ± 0.1	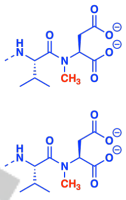
Fmoc-GGD	Weak	~ 4.4 ± 0.1 ~ 4.4 ± 0.1	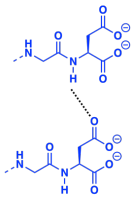
Fmoc-AVD	Strong	~ 5.8 ± 0.1 ~ 5.8 ± 0.1	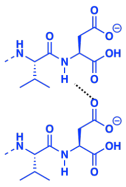

Figure 3. H-bonding of aspartic acid NH controls the pK_a shift. Schematic representation of H-bonding interaction of aspartic acid NH bond in Fmoc-AVD(NMe), Fmoc-GGD, and Fmoc-AVD assemblies. Apparent pK_a change of aspartic acid residue depends strongly on the H-bonding interaction strength of the aspartic acid NH-bond, *i.e.*, the stronger the H-bonding interaction, the higher the apparent pK_a value.

Recovering chemically fueled self-assembly

We explored whether we could tune the degree of kinetically trapping precursors in fibers by mixing Fmoc-AVD with Fmoc-GGD. We assume that both peptides coassemble and form weaker hydrogen bonds resulting in a milder shift in the pK_a of the carboxylates, thereby increasing the amount of negatively charged precursor molecules per fiber. Cryogenic transmission electron microscopy (cryo-TEM) showed that Fmoc-GGD assembled into vesicles in response to fuel (Fig. 4A), while a mixture of 25 mol% of Fmoc-AVD and 75 mol% Fmoc-GGD resulted in twisted tapes instead of vesicles; a good indication that the two coassemble. Moreover, the tapes of the mixture were more twisted than those formed by 100 mol% Fmoc-AVD, which we explain by the decrease in the ability to form flat β-sheets. Indeed, a ThT-assay showed that the maximum emission intensity observed after the addition of EDC declined with the increasing ratio of Fmoc-GGD to Fmoc-AVD (Fig. 4B; Fig. S12). This observation was further corroborated by the center of the amide-I band shifting from 1632 cm^{-1} to 1647 cm^{-1} upon gradually increasing the ratio of Fmoc-GGD to Fmoc-AVD (Fig. 4C, Fig. S13). More excitingly, the decrease in β-sheet's rigidity enabled us to tune the apparent pK_a of the precursor between 5.8 and apparent pK_a 4.4 (Fig. 4D, Fig. S5B-F). Thus, tuning the peptide content allowed us to change the microenvironment of the precursor and its degree of deprotonation. ^{1}H-NMR and fluorescence spectroscopy confirmed a decrease of kinetically trapped precursor from 48% to 18% for pure Fmoc-AVD to 50 mol% Fmoc-AVD with Fmoc-GGD content (Fig. 4E, Fig. 5A-C, Fig. S14).

This article is protected by copyright. All rights reserved.

25704206, ja, Downloaded from https://chemistry-europe.onlinelibrary.wiley.com/doi/10.1002/syst.202200035 by Cochrane Germany, Wiley Online Library on [13/10/2022]. See the Terms and Conditions (https://onlinelibrary.wiley.com/terms-and-conditions) on Wiley Online Library for rules of use; OA articles are governed by the applicable Creative Commons License

Accepted Manuscript

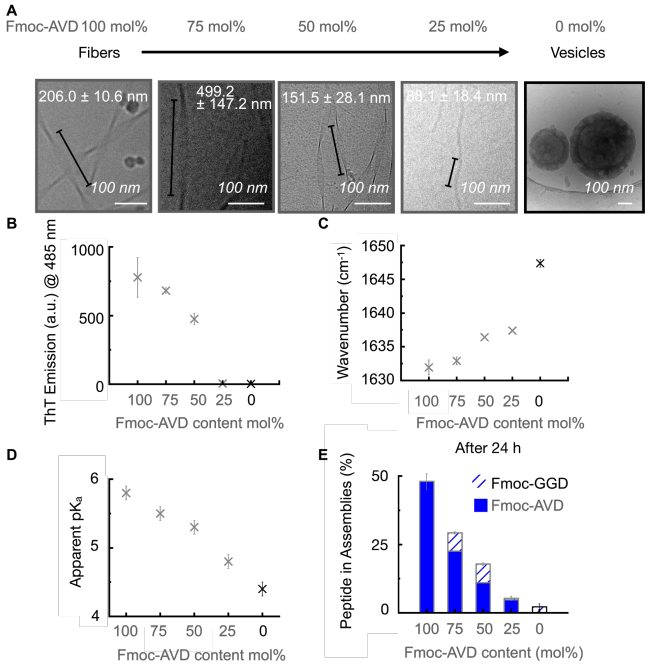

Figure 4. Changing the precursor's microenvironment through coassembly. **A)** Cryo-TEM micrographs of peptide solutions with varying Fmoc-AVD and Fmoc-GGD composition, 2 minutes after fueling with 10 mM EDC; for 100 mol% Fmoc-GGD 4 minutes after fueling with 50 mM EDC. **B)** The maximum ThT emission (a.u.) at 485 nm after excitation at 440 nm of fueled peptide solution with varying Fmoc-AVD and Fmoc-GGD composition. **C)** Maximum IR-absorption wavelength of amide I derived from FT-IR spectra of fueled peptide solution with varying ratios of Fmoc-AVD and Fmoc-GGD. The spectra were recorded after 3 minutes. **D)** The apparent pK_a values of the carboxylates of the peptides in assemblies for 10 mM total peptide concentration. **E)** The percentage of trapped precursors in the molecular assemblies after 24 hours as determined by ^{1}H-NMR for fueled peptide solutions with varying Fmoc-AVD and Fmoc-GGD composition. All error bars represent the standard deviation of the mean for n = 3.

From the combined experiments, we can create a simplified energy landscape of the transitions occurring in our chemically fueled system (Scheme 2). The peptide in this landscape can be in four states: it can be activated or not, and it can be in solution or the microenvironment of the fiber. Consequently, four reversible transitions are possible, *i.e.*, the non-assembled precursor can be activated, the activated building block can assemble, the assembled activated product can deactivate, and the deactivated precursor can disassemble. The thermodynamically most favored state is the non-activated, non-assembled peptide. Upon activation, the product assembles into a fiber. Deactivation leads to the deactivated peptide in a fiber. The disassembly of the precursor is endowed with a high energy barrier (E_b) which leads to the precursor being kinetically trapped within the fiber. Due to the kinetic trapping, the deactivated peptide is more likely to become re-activated than disassemble as shown by combined NMR and HPLC kinetics (Fig. S2A). The kinetics show that in the first 10 minutes all peptide is assembled. Thus, activation and deactivation mostly take place in the assembled state which is in line with previous work.[9f] To conclude, the peptide spends most of its time in the peptide microenvironment, where most fuel is consumed. Through changes in molecular design and pH, the E_b can be decreased.

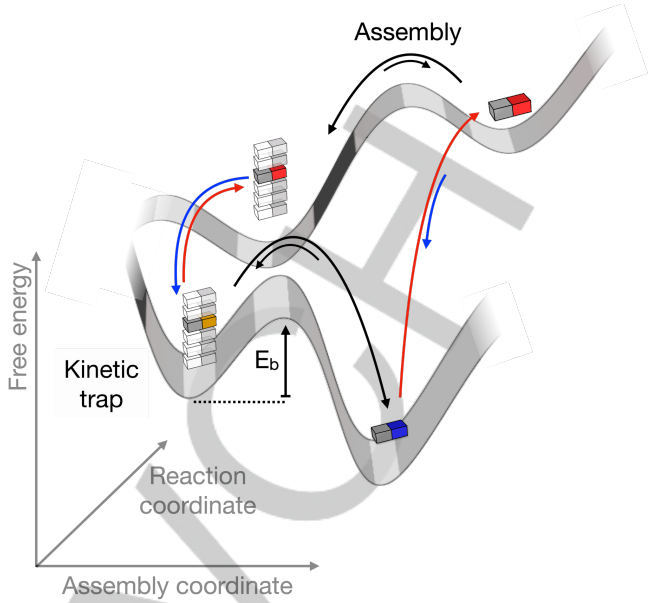

Scheme 2. Schematic and simplified representation of the free energy landscape of chemically fueled assembly.

With our increased understanding of trapping in chemically fueled assembly, we tested the dynamics of assemblies by measuring the amount of peptide in the assembly as a function of time using ^{1}H-NMR spectroscopy (Fig. 5 A-C). For assemblies of Fmoc-AVD fueled with 100 mM EDC at pH 6 and 6.5, we found that 66% and 60% of peptides remain in the assembly one hour after EDC addition. For assemblies of 50 mol% Fmoc-AVD and 50 mol% Fmoc-GGD at pH 6, the amount of trapped assembled peptide decreased to 30%. We used confocal microscopy to study the dynamics of assembly and disassembly further. We imaged several XYZ-stacks (z-dimension 5-10 μm) over time. After imaging the temporal z-stacks, we corrected for x/y-drift. We analyzed the change of the images as a function of time by calculating the Pearson correlation coefficient between sequential images of an area of 8.7 µm x 10.2 μm.[18] We calculated the Pearson correlation coefficient between frames spaced apart 10 min (Fig. 5D-F). We determined the changes of the assemblies by colocalization analysis. The Pearson correlation is 1 if the assemblies at 10 minutes and 20 minutes in the reaction cycle are identical, whereas a Pearson correlation of 0 means, the assemblies changed completely. For assemblies of Fmoc-AVD at pH 6 the Pearson correlation coefficient ranges between 0.9 and 1.0 (Fig. 5D, G). A strong correlation from image to image implies a lack of assembly and disassembly. At pH 6.5, the correlation coefficient ranged from 0.75 and 1.0, showing that the assemblies were slightly more dynamic (Fig. 5E, H). Finally, for assemblies of 50 mol% Fmoc-AVD and 50 mol% Fmoc-GGD at pH 6, the correlation coefficient range broadened to 0.25-1.0, indicating that these assemblies are more dynamic than pure Fmoc-AVD (Fig. 5F, I).

Excitingly, we observed behavior reminiscent of the dynamic instabilities of microtubules, *i.e.*, some fibers could switch from growing to collapsing and back to growing again. This behavior was only observed on fiber ends that were not embedded in a dense network of other fibers making it complicated to image these fibers due to the drifting of the sample. Thus, we trapped 2.5 mM of precursor solution in a 1.5% agarose gel and added a layer of 100 mM EDC on top of the gel. Doing ensured the fibers were in a pseudo-steady state (Fig. S15-16) and tended to drift

This article is protected by copyright. All rights reserved.

25704206, ja, Downloaded from https://chemistry-europe.onlinelibrary.wiley.com/doi/10.1002/syst.202200035 by Cochrane Germany, Wiley Online Library on [13/10/2022]. See the Terms and Conditions (https://onlinelibrary.wiley.com/terms-and-conditions) on Wiley Online Library for rules of use; OA articles are governed by the applicable Creative Commons License

Accepted Manuscript

less. We imaged the samples and followed the evolution of a fiber's length as a function of time over several z-planes (5-10 µm). For Fmoc-AVD at pH 6 or 6.5, no noticeable growth and collapse of the dangling fibers were found (Fig. 5J). For the mixture of 50 mol% Fmoc-GGD and 50 mol% Fmoc-AVD assemblies, we observed that some fiber tips alternately grew and collapsed while fuel was present (Fig. 5J, K). 3D projections of the images confirmed that the fibers were not falling in and out of the focal plane but growing and shrinking (Fig. 5K, L, Fig. S17-18, Supporting Movie M1-4). From the data in Fig. 5C and Fig. S17-18, it can be noted that fibers grow and collapse on a time scale of 0.1 - 1.4 µm/min.

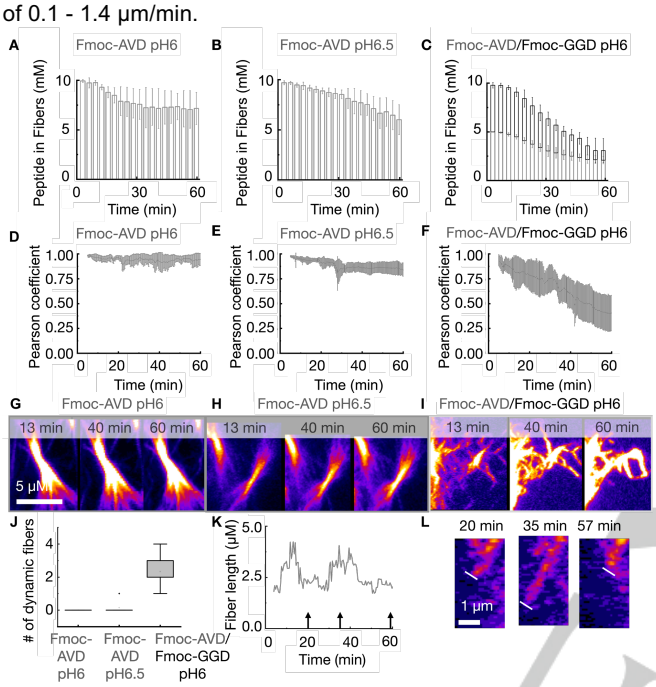

Figure 5. Dynamic self-assembly of fibers. **A-C)** The concentration of peptide in the assemblies as a function of time determined by ^{1}H-NMR spectroscopy when fueling Fmoc-AVD at pH 6 (**A**) and pH 6.5 (**B**) and Fmoc-AVD mixed with Fmoc-GGD at pH 6 (**C**). **D-F)** The correlation coefficient between two confocal micrographs taken 10 minutes apart as a function of time when fueling Fmoc-AVD at pH 6 (**D**) or pH 6.5 (**E**), and Fmoc-AVD mixed with Fmoc-GGD at pH 6 (**F**). **G-I)** Confocal micrographs, 13 min, 40 min, and 60 min after fueling **G)** Fmoc-AVD at pH 6, **H)** or pH 6.5, and **I)** Fmoc-GGD mixed with Fmoc-AVD at pH 6. Samples were stained with dye Nile Red. **J)** Number of counted dynamic fibers that grow and collapse in (18x12 µm). **K)** Fiber length as a function of time for a growing and shrinking fiber. The analyzed fiber is shown in **L)** and the supporting movie M1 and was obtained after fueling Fmoc-GGD mixed with Fmoc-AVD at pH 6. Arrows highlight the time points confocal micrographs are shown in **L)**. **L)** Confocal micrographs 20 min, 35 min, and 57 min after fueling Fmoc-GGD mixed with Fmoc-AVD at pH 6, stained with dye Nile Red. All error bars represent the standard deviation of the mean for n = 3.

Conclusion

We demonstrated how precursors remain kinetically trapped in chemically fueled fibers regulated through transient charge negation. We showed how we can tune the degree of kinetic trapping by molecular design, which yield fibers with increased dynamics. The mechanism can be exploited to design fibers that show dynamic instabilities as microtubules do in future work. These fibers can be used for adaptive biomedical and nanotechnological applications.

Acknowledgements

The BoekhovenLab is grateful for support from the TUM Innovation Network - RISE funded through the Excellence Strategy. This research was conducted within the Max Planck School Matter to Life, supported by the German Federal Ministry of Education and Research (BMBF) in collaboration with the Max Planck Society. B.A.K.K. is grateful for a Kekulé-Stipendium by the Verbandes der Chemischen Industrie. J.B. is grateful for funding from the European Research Council (ERC starting grant 852187), the Volkswagen Foundation via the Life? Program, and the Deutsche Forschungsgemeinschaft (DFG) for the funding project 411722921. Cryo-TEM measurements were performed using infrastructure contributed by the Dietz Lab and the TUM EM Core Facility. We acknowledge the technical support provided by Fabian Kohler.

Conflict of interest

The authors declare no conflict of interest.

Keywords

Dynamic instability • Dynamic fibers • Kinetically trapping • Microenvironmental change • pK_a shift

References

[1] a) A. Krissanaprasit, C. M. Key, S. Pontula, T. H. LaBean, *Chem. Rev.* **2021**, *121*, 13797-13868; b) J. Zhu, N. Avakyan, A. Kakkis, A. M. Hoffnagle, K. Han, Y. Li, Z. Zhang, T. S. Choi, Y. Na, C.-J. Yu, F. A. Tezcan, *Chem. Rev.* **2021**, *121*, 13701-13796; c) F. Sheehan, D. Sementa, A. Jain, M. Kumar, M. Tayarani-Najjaran, D. Kroiss, R. V. Ulijn, *Chem. Rev.* **2021**, *121*, 13869-13914; d) Q. Song, Z. Cheng, M. Kariuki, S. C. L. Hall, S. K. Hill, J. Y. Rho, S. Perrier, *Chem. Rev.* **2021**, *121*, 13936-13995.

[2] a) T. Aida, E. W. Meijer, S. I. Stupp, *Science* **2012**, *335*, 813-817; b) D. B. Amabilino, D. K. Smith, J. W. Steed, *Chem. Soc. Rev.* **2017**, *46*, 2404-2420; c) H. Chen, J. Fraser Stoddart, *Nat. Rev. Mater.* **2021**, *6*, 804-828; d) J. Boekhoven, S. I. Stupp, *Adv. Mater.* **2014**, *26*, 1642-1659; e) M. J. Webber, R. Langer, *Chem. Soc. Rev.* **2017**, *46*, 6600-6620.

[3] a) R. Freeman, M. Han, Z. Álvarez, J. A. Lewis, J. R. Wester, N. Stephanopoulos, M. T. McClendon, C. Lynsky, J. M. Godbe, H. Sangji, E. Luijten, S. I. Stupp, *Science* **2018**, *362*, 808-813; b) R. Merindol, A. Walther, *Chem. Soc. Rev.* **2017**, *46*, 5588-5619; c) A. Walther, *Adv. Mater.* **2020**, *32*, 1905111.

[4] a) J. Zhou, X. Du, N. Yamagata, B. Xu, *J. Am. Chem. Soc.* **2016**, *138*, 3813-3823; b) J. Zhou, X. Du, C. Berciu, H. He, J. Shi, D. Nicastro, B. Xu, *Chem* **2016**, *1*, 246-263; c) A. Sorrenti, J. Leira-Iglesias, A. Sato, T. M. Hermans, *Nat. Commun.* **2017**, *8*, 15899; d) J. Zhou, X. Du, J. Wang, N. Yamagata, B. Xu, *Front Chem Sci Eng* **2017**, *11*, 509-515; e) A. N. Shy, J. Li, J. Shi, N. Zhou, B. Xu, *J Drug Target* **2020**, *28*, 760-765.

[5] a) F. Tantakitti, J. Boekhoven, X. Wang, R. V. Kazantsev, T. Yu, J. Li, E. Zhuang, R. Zandi, J. H. Ortony, C. J. Newcomb, L. C. Palmer, G. S. Shekhawat, M. O. de la Cruz, G. C. Schatz, S. I. Stupp, *Nat Mater* **2016**, *15*, 469-476; b) M. F. Hagan, O. M. Elrad, R. L. Jack, *Chem. Phys.* **2011**, *135*, 104115; c) M. Nakagawa, S. Kai, T. Kojima, S. Hiraoka, *Eur. J. Chem.* **2018**, *24*, 8804-8808.

This article is protected by copyright. All rights reserved.

25704206, ja, Downloaded from https://chemistry-europe.onlinelibrary.wiley.com/doi/10.1002/syst.202200035 by Cochrane Germany, Wiley Online Library on [13/10/2022]. See the Terms and Conditions (https://onlinelibrary.wiley.com/terms-and-conditions) on Wiley Online Library for rules of use; OA articles are governed by the applicable Creative Commons License

Accepted Manuscript

[6] a) B. Rieß, R. K. Grötsch, J. Boekhoven, *Chem* **2020**, *6*, 552-578; b) K. Das, L. Gabrielli, L. J. Prins, *Angew. Chem. Int. Ed.* **2021**, *60*, 20120-20143; c) M. Weißenfels, J. Gemen, R. Klajn, *Chem* **2021**, *7*, 23-37.

[7] S. A. P. van Rossum, M. Tena-Solsona, J. H. van Esch, R. Eelkema, J. Boekhoven, *Chem. Soc. Rev.* **2017**, *46*, 5519-5535.

[8] a) K. Dai, J. R. Fores, C. Wanzke, B. Winkeljann, A. M. Bergmann, O. Lieleg, J. Boekhoven, *J. Am. Chem. Soc.* **2020**, *142*, 14142-14149; b) M. Tena-Solsona, B. Rieß, R. K. Grötsch, F. C. Löhrer, C. Wanzke, B. Käsdorf, A. R. Bausch, P. Müller-Buschbaum, O. Lieleg, J. Boekhoven, *Nat. Commun.* **2017**, *8*, 15895.

[9] a) J. Boekhoven, W. E. Hendriksen, G. J. M. Koper, R. Eelkema, J. H. v. Esch, *Science* **2015**, *349*, 1075-1079; b) J. Leira-Iglesias, A. Tassoni, T. Adachi, M. Stich, T. M. Hermans, *Nat. Nanotechnol.* **2018**, *13*, 1021-1027; c) S. Panja, B. Dietrich, D. J. Adams, *ChemSystemsChem* **2020**, *2*, e1900038; d) R. K. Grötsch, A. Angı, Y. G. Mideksa, C. Wanzke, M. Tena-Solsona, M. J. Feige, B. Rieger, J. Boekhoven, *Angew. Chem. Int. Ed.* **2018**, *57*, 14608-14612; e) C. Donau, F. Späth, M. Sosson, B. A. K. Kriebisch, F. Schnitter, M. Tena-Solsona, H.-S. Kang, E. Salibi, M. Sattler, H. Mutschler, J. Boekhoven, *Nat. Commun.* **2020**, *11*, 5167; f) B. A. K. Kriebisch, A. Jussupow, A. M. Bergmann, F. Kohler, H. Dietz, V. R. I. Kaila, J. Boekhoven, *J. Am. Chem. Soc.* **2020**, *142*, 20837-20844; g) C. Wanzke, A. Jussupow, F. Kohler, H. Dietz, V. R. I. Kaila, J. Boekhoven, *ChemSystemsChem* **2020**, *2*, e1900044; h) J. Boekhoven, J. M. Poolman, C. Maity, F. Li, L. van der Mee, C. B. Minkenberg, E. Mendes, J. H. van Esch, R. Eelkema, *Nat. Chem.* **2013**, *5*, 433-437; i) M. M. Hossain, J. L. Atkinson, C. S. Hartley, *Angew. Chem. Int. Ed.* **2020**, *59*, 13807-13813; j) L. S. Kariyawasam, J. C. Kron, R. Jiang, A. J. Sommer, C. S. Hartley, *J. Org. Chem.* **2020**, *85*, 682-690; k) L. S. Kariyawasam, C. S. Hartley, *J. Am. Chem. Soc.* **2017**, *139*, 11949-11955; l) P. S. Schwarz, M. Tena-Solsona, K. Dai, J. Boekhoven, *Chem. Commun.* **2022**, *58*, 1284-1297; m) W. Zeng, C. Fan, X. Xing, H. Cheng, H. Fu, B. Ma, Z. Yang, R. Zhang, W. Zhang, *Giant* **2021**, *7*, 100067; n) N. Singh, A. Lopez-Acosta, G. J. M. Formon, T. M. Hermans, *J. Am. Chem. Soc.* **2022**, *144*, 410-415; o) C. M. E. Kriebisch, A. M. Bergmann, J. Boekhoven, *J. Am. Chem. Soc.* **2021**, *143*, 7719-7725; p) S. Bal, C. Ghosh, T. Ghosh, R. K. Vijayaraghavan, D. Das, *Angew. Chem. Int. Ed.* **2020**, *59*, 13506-13510; q) S. Bal, K. Das, S. Ahmed, D. Das, *Angew. Chem. Int. Ed.* **2019**, *58*, 244-247.

[10] M. Tena-Solsona, C. Wanzke, B. Riess, A. R. Bausch, J. Boekhoven, *Nat. Commun.* **2018**, *9*, 2044.

[11] a) K. Dai, M. Tena-Solsona, J. Rodon Fores, A. M. Bergmann, J. Boekhoven, *Nanoscale* **2021**, *13*, 19864-19869; b) G. Panzarasa, A. L. Torzynski, T. Sai, K. Smith-Mannschott, E. R. Dufresne, *Soft Matter* **2020**, *16*, 591-594.

[12] F. Schnitter, J. Boekhoven, *ChemSystemsChem* **2021**, *3*, e2000037.

[13] a) C. Tang, A. M. Smith, R. F. Collins, R. V. Ulijn, A. Saiani, *Langmuir* **2009**, *25*, 9447-9453; b) D. J. Adams, L. M. Mullen, M. Berta, L. Chen, W. J. Frith, *Soft Matter* **2010**, *6*, 1971-1980; c) T. K. Harris, G. J. Turner, *IUBMB Life* **2002**, *53*, 85-98.

[14] Y. Wang, M. Lovrak, Q. Liu, C. Maity, V. A. A. le Sage, X. Guo, R. Eelkema, J. H. van Esch, *J. Am. Chem. Soc.* **2019**, *141*, 2847-2851.

[15] a) M. Biancalana, K. Makabe, A. Koide, S. Koide, *J Mol Biol* **2009**, *385*, 1052-1063; b) T. N. Tikhonova, N. N. Rovnyagina, Z. A. Arnon, B. P. Yakimov, Y. M. Efremov, D. Cohen-Gerassi, M. Halperin-Sternfeld, N. V. Kosheleva, V. P. Drachev, A. A. Svistunov, P. S. Timashev, L. Adler-Abramovich, E. A. Shirshin, *Angew. Chem. Int. Ed.* **2021**, *60*, 25339-25345.

[16] a) J. Kubelka, T. A. Keiderling, *J. Am. Chem. Soc.* **2001**, *123*, 12048-12058; bS. Krimm, J. Bandekar, *Adv Protein Chem* **1986**, *38*, 181-364.

[17] G. Cheng, V. Castelletto, C. M. Moulton, G. E. Newby, I. W. Hamley, *Langmuir* **2010**, *26*, 4990-4998.

[18] a) K. W. Dunn, M. M. Kamocka, J. H. McDonald, *Am J Physiol Cell Physiol* **2011**, *300*, C723-742; b) J. S. Aaron, A. B. Taylor, T.-L. Chew, *J. Cell Sci.* **2018**, *131*; cJ. A. Pike, I. B. Styles, J. Z. Rappoport, J. K. Heath, *Methods* **2017**, *115*, 42-54.

This article is protected by copyright. All rights reserved.

25704206, ja, Downloaded from https://chemistry-europe.onlinelibrary.wiley.com/doi/10.1002/syst.202200035 by Cochrane Germany, Wiley Online Library on [13/10/2022]. See the Terms and Conditions (https://onlinelibrary.wiley.com/terms-and-conditions) on Wiley Online Library for rules of use; OA articles are governed by the applicable Creative Commons License

Accepted Manuscript Online

10.1002/syst.202200035

WILEY-VCH

RESEARCH ARTICLE

Entry for the Table of Contents

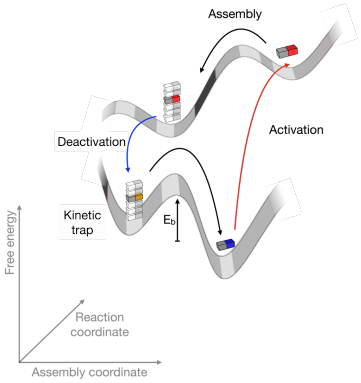

(height 5 cm; width: 4.74 cm)

Dynamic molecular self-assemblies like microtubules show dynamic instabilities. Synthetic analogs of such dynamic assemblies regulated by chemical-fueled reaction cycles often face the challenge to display dynamic instability. In this work, we show how molecular design can be used to tune the degree of kinetically trapping to approach dynamic instability.

Researcher Twitter usernames: @BoekhovenLab; @B_Kriebisch; @CKriebisch

This article is protected by copyright. All rights reserved.

25704206, ja, Downloaded from https://chemistry-europe.onlinelibrary.wiley.com/doi/10.1002/syst.202200035 by Cochrane Germany, Wiley Online Library on [13/10/2022]. See the Terms and Conditions (https://onlinelibrary.wiley.com/terms-and-conditions) on Wiley Online Library for rules of use; OA articles are governed by the applicable Creative Commons License

Accepted Manuscript